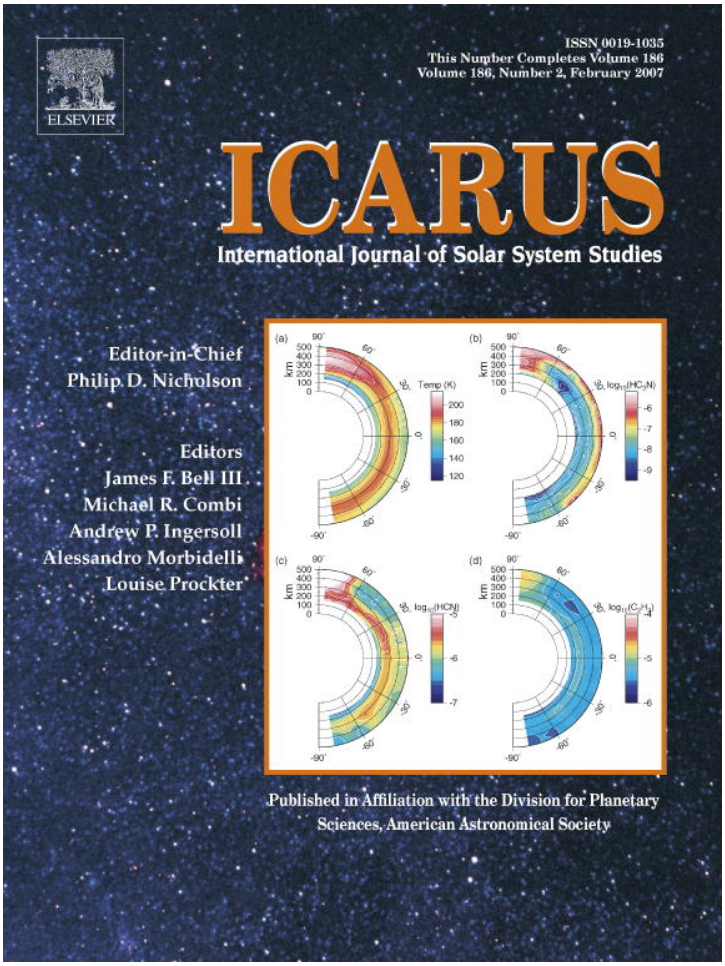

Available online at www.sciencedirect.com
ScienceDirect
Icarus 186 (2007) 571–580
ICARUS
www.elsevier.com/locate/icarus

Solar radiation acceleration effects on Mercury sodium emission

A.E. Potter [a,*], R.M. Killen [b], T.H. Morgan [c]

[a] National Solar Observatory, P.O. Box 26732, 950 N. Cherry Avenue, Tucson, AZ 85726-6732, USA
[b] Department of Astronomy, University of Maryland, College Park, MD 20742-2425, USA
[c] NASA Headquarters, 300 E Street SW, Washington, DC 20546-0001, USA

Received 23 May 2006; revised 21 September 2006

Available online 22 November 2006

Abstract

A set of Mercury sodium emission data collected over a range of true anomaly angles during 1997–2003 was used to analyze the effect of solar radiation acceleration on sodium emissions. The variation of emission intensity with changing Doppler velocities throughout the orbit was minimized by normalizing the intensities to a constant true anomaly angle. The normalized intensities should be independent of orbital position if sodium density is constant. Plots of the normalized intensities against solar radiation acceleration showed very considerable scatter. However, the scatter was not random, but the result of a systematic variation, such that the normalized emission at a particular value of radiation acceleration took one or the other of two values, depending on the value of the true anomaly angle. We propose that this was the result of solar radiation acceleration changing the velocity of the sodium atoms, and consequently changing the solar continuum seen by the atoms. There is a positive feedback loop in the "out" leg of the orbit, such that radiation acceleration increases the solar continuum intensity seen by the atoms, and a negative feedback loop in the "in" leg of the orbit, such radiation acceleration decreases the continuum intensity. The observations could be approximately fit by assuming that sodium atoms are exposed to sunlight for an average of 1700 s. The emission values corrected for this effect showed much less scatter, with a general trend of about 30% to lower values from minimum to maximum radiation acceleration. The corrected emissions were used to calculate average column densities, and the result compared with the predictions of Smyth and Marconi [Smyth, W.H., Marconi, M.L., 1995. Astrophys. J. 441, 839–864] for the variation of column density with true anomaly angle. The comparison suggests that sodium atoms interact weakly with the surface. The effect of radiation acceleration on emission intensities should be taken into account if column densities are to be calculated from emission intensities.

Keywords: Mercury; Atmospheres, dynamics; Atmospheres, structure

1. Introduction

Sodium atoms in the exosphere of Mercury are subject to large solar radiation accelerations as a consequence of the large radial velocities experienced by Mercury in the course of its elliptical orbit. The radial velocity of Mercury swings between −10.06 and +10.06 km/s, and as a result, the solar continuum seen by a sodium atom Doppler shifts in the range between +200 and −200 milliangstroms from the center of the sodium Fraunhofer line in the solar spectrum. The solar intensity seen by a sodium atom changes slightly more than an order of magnitude in the range from minimum to maximum radial velocity, with a corresponding change in the solar radiation acceleration experienced by the atoms. The resonance transition of the sodium atom at the D lines is very strong, and as a result, the radiation acceleration is large, reaching 54% of surface gravity at the maximum radial velocity of Mercury.

It is reasonable to expect that solar radiation acceleration should affect the distribution of sodium on the planet, and several theoretical studies have considered this. Smyth (1986) and Smyth and Marconi (1995) showed that lateral (anti-sunward) transport of sodium atoms driven by radiation acceleration is competitive with the photoionization lifetime of sodium over a significant portion of the orbit, and could lead to the loss of sodium from the planet. Ip (1990) showed that radiation acceleration should lead to the transport of sodium to the terminator, and its accumulation there. Observational evidence as

* Corresponding author.
E-mail address: apotter@noao.edu (A.E. Potter).

0019-1035/$ – see front matter
doi:10.1016/j.icarus.2006.09.025

to the effect of radiation acceleration is contradictory. Potter and Morgan (1987) found that the average column density of sodium decreased as solar radiation acceleration increased, as might be expected from the theoretical models. However, later work by Sprague et al. (1997) failed to find evidence for an effect of radiation acceleration on the sodium density. Potter et al. (2002) observed an anti-sunward sodium tail of the planet at high values of radiation acceleration, confirming the prediction of Smyth and Marconi (1995). In this paper, the effect of radiation acceleration on Mercury sodium is approached using a data set accumulated during 1997–2003 using the McMath–Pierce Solar Telescope at the Kitt Peak National Observatory. The sodium emission images from this data set showed variations in the distribution of sodium over the planet, and an analysis of the spatial distributions has been published (Potter et al., 2006). Some of the data have been used to calculate the planet-average sodium abundances (Killen et al., 2004). As will be seen later in this paper, the estimation of abundances from emission intensities requires a correction for radiation acceleration. That correction was not applied to those data, so they should be regarded as preliminary.

2. Observations

Our observations of Mercury were done at the McMath–Pierce Solar Telescope using an image slicer having a 10-arcsec square aperture, large enough to view the entire disk of Mercury. Since 1997, we have used this arrangement to view Mercury during each year up to 2003, eventually covering a nearly complete range of true anomaly angles for the planet.

The output from the slicer was sent through the Stellar Spectrograph to an 800 × 800 element CCD where the spectral–spatial image was recorded. All the observations were done during daylight, with exposures in the range 30 to 45 s. Each observation with Mercury in the field of view was followed by an observation of the sky about 30 arcsec away from Mercury. The Mercury spectrum was obtained by subtraction of the sky spectrum from the Mercury plus sky spectrum. Flat-fielding was done using an averaged sky spectrum. Sodium emission values were extracted from each spectrum assuming the continuum under the emission line to follow a quadratic equation whose constants were determined from two points of the continuum signal on either side of the emission line. The sodium emission signals were rearranged to form 10 × 10-arcsec images having 1-arcsec pixels for both the sodium emission and sunlight reflected from the planetary surface. On average, Mercury was about 6 arcsec in diameter at the time of observation, and most of the observations were made near phase angles of 90°. With seeing of the order of 2 arcsec, we estimate that the 10 × 10-arcsec slicer captured 90% or better of the sodium emission.

2.1. Calibration and noise

The sodium emission intensities were calibrated from the intensity of sunlight reflected from the Mercury surface, using reflectance values derived from a Hapke reflectance model. There are several reflectance models for Mercury in the literature. Domingue et al. (1997) compared six different models for the bidirectional reflectance of Mercury's surface, finding differences up to ±30%. The greatest difference was found between solution 3 (Ververka et al., 1998) and solution 6 (Domingue et al., 1997), both of which used extreme estimates for surface albedo and surface roughness. Since then, Mallama et al. (2002) have published a Hapke model for Mercury's surface reflectance based on observations of the planet Mercury by SOHO. This model appears to be the best choice for this data set, considering that these measurements did not require corrections for atmospheric effects and covered a very wide range of phase angles. In any case, the conclusions from analysis of this data set do not depend critically on the absolute surface reflectance because the values of sodium emission are compared relative to one another. There is no evidence that one half of the planet is consistently brighter than the other. Any error in the surface reflectance is systematic and not random.

The calibration procedure (described also by Sprague et al., 1997 and Potter et al., 1999) was as follows: A Hapke reflection image of the planet was generated for the phase of the observation (using the optical constants from Mallama et al., 2002), and then convolved with Gaussians of varying widths, until the image matched the observed surface reflection image. The peak reflectivity in this convolved image was used with the peak signal intensity in the observed image to get a calibration constant in terms of kilorayleighs. This procedure also yielded a value for the seeing, derived from the width of the Gaussian, which is useful for determining the quality of the image.

There were a total of 102 useful observing days in the 1997–2003 period. Each day, yielded from three to a hundred images. In the end, there were 38 days which had the dusk terminator exposed to observation, and 64 days for which the dawn terminator was exposed. The quality of the images varied, depending on seeing conditions during the observation. The seeing, defined as the Gaussian sigma, ranged from about 1.6 to 4 arcsec, with an average of 2.7 arcsec over the whole data set. In order to exclude the worst images in any given observation day, images were rejected if they showed seeing levels greater than 0.7 arcsec larger than the best seeing level on that day. The final total data set included approximately 800 images of the sodium emission from Mercury. The planet-wide average for each image was determined by summing the sodium emissions from each 1-arcsec pixel in the image, and dividing by the number of pixels in the image (100). While the 10 × 10-arcsec field of view of the slicer is larger than the angular size of Mercury during the observations, seeing blur expands the Mercury image such that not all of the planet will be in the field of view. Consequently, not all the sodium emission from the planet will be captured by the slicer, with the result that the average values will be smaller. For a typical view of Mercury (6 arcsec diameter, phase angle 90°), 15% of the emission is lost for seeing of 2 arcsec, and about 25% for seeing of 3 arcsec. For the overall average seeing of 2.7 arcsec for this data set, the sodium emissions as observed would be about 20% smaller than the true values. The standard deviation of the planet-wide average sodium D_2 emission on any given day averaged about 10% of

the mean value, with most of the scatter resulting from seeing variations. The essential elements of the data set are recorded in Table 1. Phase angles when the dusk terminator of Mercury is in view are defined as 360 minus the conventional phase angle.

2.2. Phase angle effects on the average emission

These observations were made at a variety of phase angles. For a uniform exosphere, the intensity of scattered sunlight varies across the planetary disk, becoming bright at the limb. As the phase angle increases, the bright limb occupies more and more of the field of view, with a resulting increase of the average emission value. This effect must be taken into account in order to compare averages from different observations. Since the distribution of sodium over the surface varies, it is not possible to make an exact correction of this data set. However, an approximate correction can be applied, and this was thought to be better than no correction. For this purpose, sodium was assumed to be uniformly distributed over the surface, and the average sodium emission over the visible planet was calculated as a function of phase angle for optical depths in the range from 0.1 to 2.0. The effective optical depth for this data set was estimated from the average ratio of D_2 to D_1 emissions, which was 1.61 ± 0.31 (corrected for the different solar intensities in the two Fraunhofer lines). A reasonable value for optical depth corresponding to this ratio is 0.1. Consequently, all the average sodium emission intensities were corrected to a phase angle of 90° using the factors for optical depth 0.1 shown in Table 2. The corrections are not more than 16%, except for phase angles greater than 120°, of which there are two data points. The scatter of the data is reduced, with better correspondence between observations having the dawn terminator in view with those with the dusk terminator in view.

3. Variation of average sodium emission with true anomaly angle

The average sodium D_2 emission intensities are plotted against true anomaly in Fig. 1. We also measured the D_1 emissions, but chose not to show them, as the signal is weaker, and correspondingly, the noise is larger. The analysis of spatial distribution of sodium on Mercury (Potter et al., 2006) showed that there are differences between observations that view the dawn terminator and those that view the dusk terminator. Consequently, these two conditions are differentiated in the plot. The theoretical D_2 emission rate for a sodium atom in terms of photons/s atom (the g-factor) is also plotted. For a constant amount of sodium in the exosphere (at rest with respect to the planet), the observed emission intensity should vary with true anomaly angle exactly the same as the g-factor, and this is approximately the case. However, there are some differences. There is a difference between the dawn side and the dusk side for true anomalies near 90°, in that the dawn side emission intensities are larger than for the dusk side. The observed peak values for the dawn side do not occur precisely at the calculated peak. For true anomaly angles less that 180° (Mercury moving outward from the Sun), there is an emission peak just before the calculated maximum and another peak just after the calculated maximum. For true anomaly angles greater than 180° (Mercury moving inward), the emission peak occurs just before the calculated maximum.

3.1. The normalized average sodium emission

The Doppler shift of the solar Fraunhofer lines as Mercury moves in its orbit can mask the changes that take place in the amount of sodium in the exosphere. It is essential to minimize the effect of the Doppler shift on the emission intensity in order to examine the effect of radiation acceleration. One approach would be to calculate the amount of sodium atoms from the emission intensities, taking into account the Doppler shifts, as has been done in previous publications (Sprague et al., 1997 and Potter et al., 1999). However, as will be shown later in this paper, this method does not take into account the effects of radiation acceleration, and can yield incorrect values for column densities. Consequently, we chose not to calculate the sodium densities, but rather chose to make the correction by normalizing all the average emission values to a single radial velocity and solar distance, i.e., to a single true anomaly. By making this correction, the sodium atoms at each true anomaly angle see exactly the same solar photon flux. If the sodium density were to be exactly the same throughout the Mercury orbit, the normalized emission would also be exactly the same. The intensities were corrected to conditions prevailing on December 9, 2000 at 00:00 UT—namely 0.45101218 AU and 5.03119 km/s radial velocity. These conditions correspond to a Doppler shift of −98.9 mA and a true anomaly angle of 150.26°. The g-factors (theoretical emission rates) for this configuration are 6.188 photons/s atom for D_1 and 9.712 photons/s atom for D_2 emissions. In the absence of any other effects, the normalized sodium emission would be proportional to the amount of sodium in the exosphere except for an underestimate of sodium density at the bright limb where the D_2 transition can be optically thick. Results of the normalization to a single true anomaly angle are shown in Fig. 2, where the normalized average D_2 emission is plotted against true anomaly angle.

The largest values of the normalized emission are clustered near aphelion and perihelion, rather than around the locations of maximum radiation acceleration as in Fig. 3. This might suggest that the total amount of sodium visible in the exosphere reaches maxima near perihelion and aphelion, and the maxima are about the same at the two orbital locations. However, the effects of solar radiation acceleration on the emission intensity have not been taken into account. That will be done in the following paragraphs.

4. Variation of normalized sodium emission with solar radiation acceleration

As noted above, Potter and Morgan (1987) found that the average column density of sodium decreased as solar radiation acceleration increased, but later work by Sprague et al. (1997) failed to find evidence for any effect of radiation acceleration. Both data sets were relatively small, so that the larger data set

Table 1
Observations of sodium on Mercury, 1997–2003

Date	Obs. D_2 (kR)	Obs. std. dvn. (kR)	Nrmlzd. D_2 (kR)	Nrm. std. dvn. (kR)	Phase angle (°)	True anomaly (°)	Rad. acc. (cm/s^2)	Terminator	Seeing (arcsec)
1997									
Apr 5	974	185	254	48	99.2	58.2	177.7	Dawn	3.3
Apr 6	1314	145	338	37	103.6	63.9	180.2	Dawn	3.3
Apr 7	1200	241	318	64	107.9	69.0	174.7	Dawn	3.3
Jul 15	1003	140	371	52	59.4	116.0	125.3	Dawn	3.3
Jul 16	1218	82	484	33	61.3	119.6	116.9	Dawn	3.3
Nov 13	168	7	139	6	41.7	213.4	57.1	Dawn	2.8
Nov 14	333	38	238	27	43.3	216.4	65.6	Dawn	4.2
Nov 15	428	25	263	15	45	219.5	76.2	Dawn	6.3
Nov 16	460	212	252	116	46.7	222.6	85.1	Dawn	3
Nov 18	721	79	352	38	50.3	229.0	95.2	Dawn	3.7
Nov 20	817	30	359	13	54.3	235.9	105.6	Dawn	4
1998									
Jun 1	1035	55	342	18	326.4	311.1	162.9	Dusk	3.2
Jun 2	1139	43	393	15	330	316.8	155.3	Dusk	1.6
Jun 13	1157	33	800	23	14.4	24.9	67.6	Dawn	3.3
Jun 14	1289	293	627	142	18.6	31.0	97.5	Dawn	3.3
May 29	1662	203	516	63	316.7	294.9	173.7	Dusk	3.3
May 30	1299	78	407	24	319.9	300.1	171.8	Dusk	3.5
May 31	995	309	318	99	323.2	305.5	168.5	Dusk	3.3
Nov 5	625	11	304	6	61.4	229.7	95.6	Dawn	4
Nov 6	645	192	288	86	63.3	233.0	103.5	Dawn	4
Nov 7	667	59	277	24	63.6	236.4	103.8	Dawn	2.7
Nov 8	827	26	335	11	67.8	239.9	113.8	Dawn	3.8
Nov 13	983	29	321	9	81.5	258.7	140.7	Dawn	2.9
Nov 14	1190	102	365	31	84.6	262.8	149.6	Dawn	2.9
1999									
Aug 21	214	15	301	22	292	348.1	37	Dusk	3.5
Aug 22	244	22	446	41	296.5	354.4	28.7	Dusk	1.8
Aug 23	364	60	753	123	301.6	0.2	25.2	Dusk	2.5
Aug 24	301	20	583	39	305.7	6.5	27	Dusk	2.2
Aug 25	395	72	650	118	310.7	12.8	32.3	Dusk	2.5
Aug 26	497	22	597	26	314.6	19.1	44.7	Dusk	2.3
Aug 27	817	0	661	0	319.3	25.3	67.3	Dusk	3.3
Aug 29	1600	321	680	137	327	37.4	129.2	Dusk	2.5
Aug 30	1221	89	420	31	331.4	43.2	141.9	Dusk	2.7
Aug 31	1385	145	446	47	334.4	48.9	166.9	Dusk	2.7
Jan 30	221	50	134	30	351.7	223.1	85.5	Dusk	1.9
Jan 31	185	28	102	16	352.77	226.3	87	Dusk	3.4
Nov 20	623	65	505	52	215.8	6.7	27	Dusk	2.2
Sep 1	1306	119	399	36	338.5	54.4	171.6	Dusk	2.8
2000									
Feb 5	1522	260	407	70	47.2	300.8	172.9	Dawn	2.4
Feb 6	1633	130	444	35	50.8	306.2	169.4	Dawn	2.7
Jun 1	1229	146	399	48	85.3	109.9	143.5	Dawn	2.3
Jun 2	1799	151	604	51	88.4	105.8	138.6	Dawn	1.9
Jun 3	1264	123	435	42	90.4	109.7	135.5	Dawn	2.4
Jun 4	1692	548	622	202	93	113.4	126.9	Dawn	1.9
Jun 5	1000	224	377	84	95.5	117.0	123.5	Dawn	2.2
May 30	1548	138	458	41	79.9	93.6	157.8	Dawn	2.1
May 31	1558	172	475	53	82.4	97.8	153.4	Dawn	2.4
Nov 28	569	48	249	21	322.3	117.3	123.6	Dusk	3.3
Nov 29	700	93	327	43	324.3	120.8	115.4	Dusk	3.3
2001									
Feb 4	619	91	521	76	125.8	20.2	55	Dawn	3.3
Feb 5	1051	131	603	75	132	26.4	82.1	Dawn	1.9
Mar 6	332	126	324	123	267.6	149.6	47.5	Dusk	3.7
Mar 8	305	12	454	18	271.8	155.4	31.6	Dusk	1.9
Nov 6	889	157	278	49	309.5	81.1	173.2	Dusk	2.8

(*continued on next page*)

Table 1 (*continued*)

Date	Obs. D_2 (kR)	Obs. std. dvn. (kR)	Nrmlzd. D_2 (kR)	Nrm. std. dvn. (kR)	Phase angle (°)	True anomaly (°)	Rad. acc. (cm/s^2)	Terminator	Seeing (arcsec)
Nov 7	800	223	259	72	312.8	85.7	167.4	Dusk	2.8
Nov 8	682	19	228	6	315.6	90.1	162.4	Dusk	3.4
Nov 9	774	77	267	27	318.4	94.4	157.4	Dusk	3
Sep 8	92	10	372	41	64.4	178.0	11.2	Dawn	2.4
Sep 9	242	7	1002	27	65.8	180.8	11	Dawn	2.3
Sep 10	267	35	1104	144	67.3	183.5	11.1	Dawn	1.8
Sep 11	126	12	500	50	68.7	186.3	11.6	Dawn	2.5
2002									
Aug 10	819	5	400	3	51.7	131.6	96.1	Dawn	2.9
Aug 12	491	89	302	55	54.8	138.0	77	Dawn	3
Aug 20	326	20	741	44	66.5	161.7	20.3	Dawn	2.2
Aug 21	287	44	788	122	68	164.5	16.7	Dawn	2.5
Aug 22	168	56	536	179	69.5	167.3	14.3	Dawn	2.9
Aug 23	197	20	701	72	71	170.1	14.2	Dawn	2.9
Aug 24	189	17	675	61	72.5	172.9	12.7	Dawn	2.1
Aug 25	199	14	766	53	72.5	175.6	12.7	Dawn	2.7
Feb 19	561	1	418	1	276.9	144.0	66.2	Dusk	3
Jan 4	1018	146	283	40	53.3	277.2	166.4	Dawn	3
Jan 5	1606	210	447	59	56.5	281.9	166.3	Dawn	1.9
Jan 6	1707	168	459	45	59.9	286.7	172.1	Dawn	1.9
Dec 18	823	8	256	2	53.6	260.4	148.5	Dawn	3.1
Dec 19	954	11	290	3	55.8	264.6	152.2	Dawn	5.4
Dec 20	841	17	247	5	58.9	268.9	157.2	Dawn	3.3
May 2	1446	69	406	19	99.9	86.0	166.8	Dawn	3.1
May 3	1480	65	428	19	103.4	90.4	161.6	Dawn	3
May 4	1408	184	420	55	106.6	94.7	156.8	Dawn	2.4
May 5	1718	170	530	52	110.5	98.8	151.3	Dawn	1.9
Oct 19	651	42	205	13	303.2	56.6	170	Dusk	2.1
2003									
Apr 6	469	33	576	40	59.9	15.7	37.3	Dawn	1.9
Apr 7	982	70	829	59	64.4	22.0	54.9	Dawn	1.9
Apr 8	1327	78	764	45	68.9	28.1	81.9	Dawn	1.9
Apr 9	1622	117	680	49	73.3	34.1	113.4	Dawn	1.9
Apr 10	1726	96	640	36	77.7	40.1	127.8	Dawn	2
Apr 11	1677	146	506	44	82.1	45.8	155.3	Dawn	2
Apr 13	1595	155	437	43	90.6	56.9	169.8	Dawn	2.2
Aug 10	178	17	635	62	82.7	170.4	12.8	Dawn	1.9
Aug 2	697	38	587	32	70.2	147.5	56.4	Dawn	1.9
Aug 3	766	64	767	64	71.8	150.5	47.4	Dawn	1.9
Aug 4	577	49	697	59	73.3	153.4	39	Dawn	1.9
Aug 5	437	44	647	66	74.8	156.3	31.5	Dawn	2.7
Aug 6	390	17	717	32	76.4	159.2	25.2	Dawn	2.3
Aug 7	291	23	662	52	78	162.0	20.3	Dawn	2
Aug 8	237	27	651	75	79.5	164.8	16.7	Dawn	1.9
Aug 9	179	9	600	30	278.9	167.6	14.3	Dawn	2
Dec 13	1799	119	469	31	93.8	298.1	177.6	Dawn	3.3
Dec 14	1328	317	351	84	98.6	303.5	175.5	Dawn	2.3
Feb 3	497	15	289	9	283.2	135.0	86.5	Dusk	3.3
Feb 6	491	8	348	6	289.3	144.4	70.7	Dusk	3.5
Feb 8	420	48	470	54	292.9	150.3	47.4	Dusk	4.7
Oct 1	1862	208	1074	120	66.34	28.5	81.7	Dawn	1.9
Sep 27	130	54	232	97	273.8	3.5	25.8	Dawn	1.9
Sep 28	388	74	639	123	279	9.8	29	Dawn	3
Sep 29	583	72	773	96	284	16.1	37.3	Dawn	1.9
Sep 30	981	0	915	0	288.9	22.3	54.8	Dawn	1.9

in this work could clarify the issue. For this, we have plotted the normalized average sodium emissions for our entire data set against radiation acceleration in Fig. 3.

There is a trend to smaller values as the radiation acceleration reaches its largest values near 180 cm/s^2. The average value of the normalized emission decreases about 30% from low radiation acceleration up to the maximum radiation acceleration, suggesting that sodium is lost from view, either by moving to the dark side, or off the planet altogether. This is consistent with the observation of a sodium "tail" observed near

Table 2
Phase angle correction for optical depth 0.1

Phase angle (°)	Correction to 90°
0.0	0.98
20.0	1.13
40.0	1.16
60.0	1.13
80.0	1.06
90.0	1.00
120.0	0.75
140.0	0.53

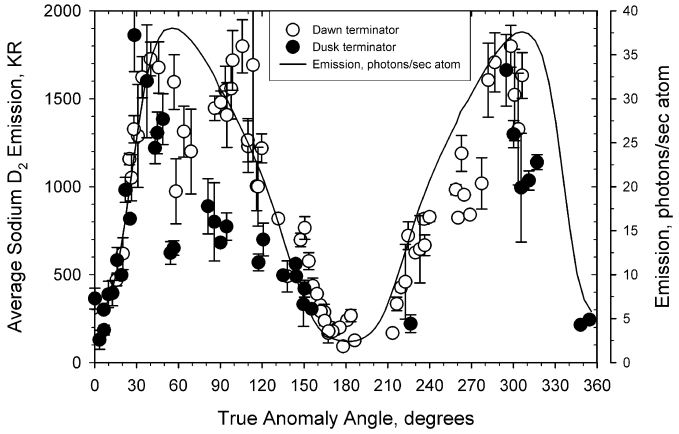

Fig. 1. Planet-wide average sodium is plotted against true anomaly angle. Dawn side observations of sodium D_2 emission are shown as open circles, and dusk side observations as filled circles. The solid line is the D_2 emission rate calculated for a single sodium atom in terms of photons/s atom (the *g*-factor), which is directly proportional to the value of solar radiation acceleration. The emission values reach minima near aphelion and perihelion, in general agreement with predicted behavior. For true anomaly angles less than 180°, there are two emission peaks, one before and one after the region of predicted maximum emission rate. For true anomaly angles greater than 180°, the observed emissions peak before the predicted maximum. There are insufficient data beyond the predicted maximum to say whether or not a second peak would appear. The ratio of maximum to minimum emission values is slightly more than an order of magnitude.

maximum radiation acceleration (Potter et al., 2002), whereby sodium is seen to be lost from the planet, forming a 60,000-km-long "tail." However, in the intermediate region, the data do not appear to follow any kind of consistent trend.

By selecting a smaller set of data, the origin of much of this scatter can be seen. An example is shown in Fig. 4, where the dawn-side emission intensities for true anomaly angles smaller than 180° observations are plotted against radiation acceleration in order of true anomaly angle, i.e., in order of orbital position. Lines are drawn between successive true anomaly angle points in the orbital track. The arrows on the figure show the direction of increasing true anomaly angle. The lines show that the data fall on a loop.

The value of the average emission depends not only on radiation acceleration, but also on orbital position, leading to a kind of hysteresis effect, whereby the emission value depends both on radiation acceleration and also on the true anomaly angle. This can be explained from the interaction of solar radiation acceleration with motion of Mercury in its orbit.

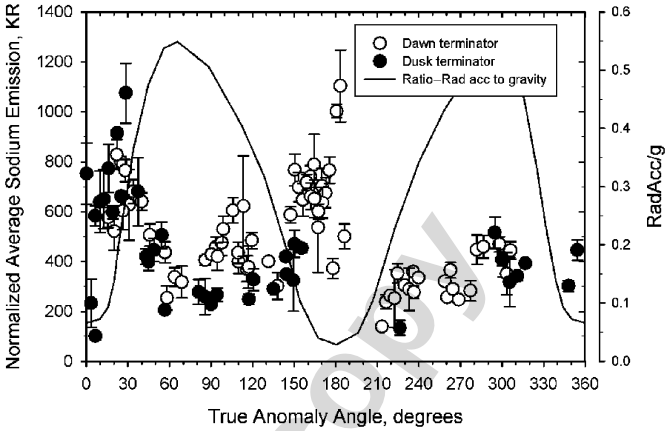

Fig. 2. To eliminate the effect of the Doppler shift on solar flux at the rest frequency of atoms in Mercury's exosphere, the emission was normalized to conditions at true anomaly angle 143.78°. The resulting emission values would be proportional to the average column abundance of sodium in the absence of acceleration effects of solar radiation. For true anomaly angles less than 180°, the normalized emission is anti-correlated with radiation pressure. For true anomaly angles greater than 180°, the variation of average emission is less clear cut, but in general, the normalized emission intensity is lower in the regions of high radiation acceleration than at aphelion and perihelion.

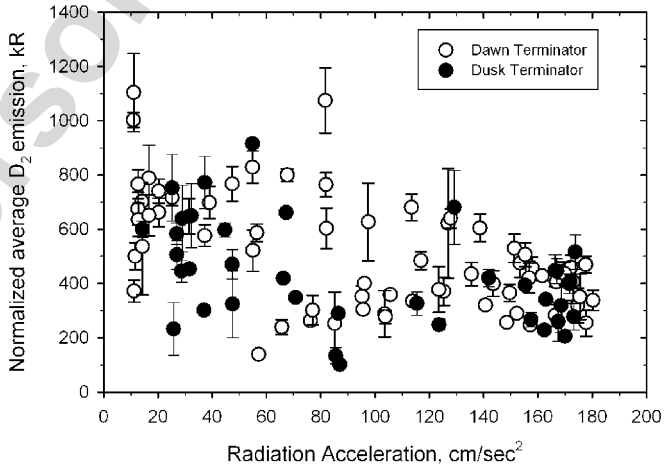

Fig. 3. The normalized sodium D_2 emission versus radiation acceleration. Dawn terminator observations are shown as open circles and dusk terminator observations as filled circles. There is a wide scatter of the data. A linear fit to the data yields an *R*-square value of 0.2.

4.1. Predicted effects of solar radiation acceleration on sodium emission intensity

When Mercury is on the "out" leg of its orbit, the sodium atoms in the Mercury exosphere see sunlight shifted redwards, and will scatter sunlight from the low-wavelength, or "blue" side of the Fraunhofer line. When the atom velocity increases as a result of radiation acceleration, the solar spectrum seen by the atom will shift further redwards, resulting in an increase of the intensity of sunlight seen by the sodium atom on the blue side of the Fraunhofer profile. This is a self-accelerating process—the faster the sodium moves anti-sunward, the greater the intensity of sunlight it sees, the greater the radiation acceleration, and the greater the intensity of scattered sunlight.

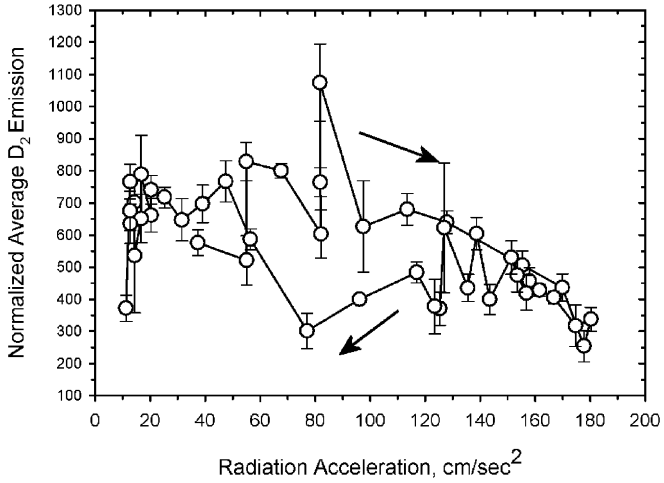

Fig. 4. A small set of normalized emission data is shown. The dawn terminator is in view, and the true anomaly angle is in the range 0° to 180° (perihelion to aphelion). Lines connecting consecutive true anomaly angles are drawn between the points, with arrows indicating the direction of increasing true anomaly angle. The data points form a loop, whereby the normalized emission intensity for a given radiation acceleration has two possible values, depending on the value of the true anomaly angle.

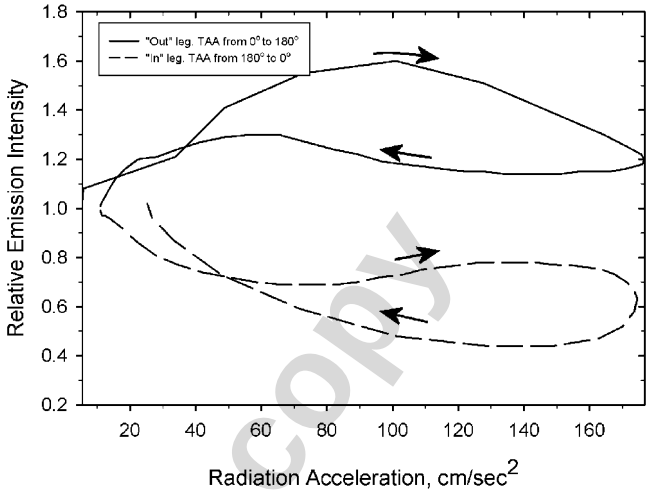

Fig. 5. Solar radiation acceleration affects emission intensity because the accelerated atoms see a different level of the solar continuum. The ratio of intensity after 1700 s of acceleration to the intensity before acceleration is shown. The solid line is the path for true anomalies in the range 0° to 180°, where radiation acceleration adds to the velocity of the sodium atoms relative to the Sun, resulting in an increase in emission. The dashed line is the path for true anomalies in the range 180° to 360°, where radiation acceleration subtracts from the velocity of the sodium atoms relative to the Sun, resulting in a decrease in emission.

When Mercury is on the "in" leg of its orbit, the situation is reversed. Here, sunlight seen at Mercury is shifted bluewards, and sodium scatters light from the high-wavelength side, or "red" side of the Fraunhofer line. Now, when radiation acceleration imparts an anti-sunward velocity to the sodium atom, the solar spectrum seen by the atom will shift redward, and the atom will see a lower intensity of sunlight. As a result, the intensity of sunlight scattered from the sodium atom decreases.

These effects were first pointed out by Smyth (1986), who predicted that solar radiation acceleration effects would produce significant differences in the emission from the sodium exosphere on the "out" leg of the orbit as compared to the "in" leg of the orbit. Detailed model calculations of the sodium exosphere by Smyth and Marconi (1995) included these effects, showing how the predicted shape of the sodium exosphere might differ between the two legs of the orbit.

After production from the surface, sodium atoms travel in ballistic trajectories over the surface, hopping from point to point until their energy is lost to the surface and they condense, or they are photoionized. Photoionization times range from about 4.6 to 10.6 h from perihelion to aphelion (Cremonese et al., 1997). Thus, a sodium atom can experience solar radiation acceleration over a period of several hours before photoionization removes it from the scene. During this time, solar radiation acceleration will change the anti-sunward velocity of the atoms, with corresponding changes in the intensity of scattered sunlight. The planet-wide interaction of solar radiation acceleration with sodium atoms is complex, with atoms generated near the subsolar point affected differently than atoms generated near the terminator. A detailed analysis of this process is beyond the scope of this paper. We anticipated that the overall effect of radiation acceleration might be described by a single number, representing the effective time that sodium atoms were exposed to sunlight, and calculated the effect for a range of exposure times. The observations could be approximately reproduced for an exposure time of 1700 s. Fig. 5 shows how the calculated relative emission intensities for sodium atoms on Mercury would vary with radiation acceleration for both the sunward and anti-sunward directions of the orbit, assuming an exposure time 1700 s. The relative intensity plotted in Fig. 5 is defined as the ratio of emission intensity after acceleration to the intensity before acceleration. The variation of relative intensity with radiation acceleration for the "out" leg of the orbit shows the expected increases in intensity resulting from increased anti-sunward velocity. The general shape of the plot corresponds approximately to the variation of the normalized average intensities plotted in Fig. 4. The variation for the "in" leg shows the expected decreases in intensity resulting from reduction of the anti-sunward velocity of the atoms.

4.2. *Comparison of model predictions with observations*

The observations are compared with the model predictions in Figs. 6 and 7. For these plots, the predicted ratios shown in Fig. 5 were multiplied by 400 kR in order to scale them to match approximately the observed values. The variation of emission intensity with radiation acceleration is somewhat different between dawn-side and dusk-side observations, so that Fig. 6 shows the comparison for dawn-side observations on the "out" and the "in" legs of the orbit respectively, and Fig. 7 shows the comparison for dusk-side observations on the "out" and "in" legs of the orbit, respectively. Arrows drawn on the figures show the increasing direction of the true anomaly angle. There is a rough correspondence between the observed and calculated values in all cases.

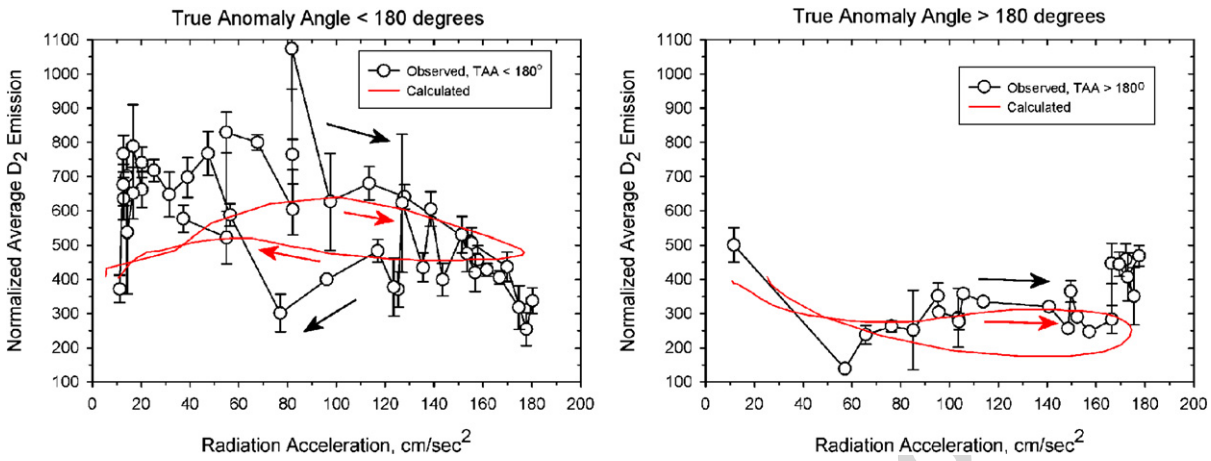

Fig. 6. The dawn terminator data shown in Fig. 3 are shown with overlay plots of calculated emission values. The left-hand part of the figure shows data for TAA values less than 180°, and the right-hand part shows data for TAA values greater than 180°. To get calculated emission values, the ratios derived from Fig. 5 were multiplied by 400 kR so as to get an approximate match between the observed and calculated variations with radiation acceleration.

4.3. Correction of the observations for radiation acceleration effects

The effect of solar radiation acceleration is to change the solar continuum level seen by a sodium atom, with the result that the emission intensity changes without any change in the column density of sodium atoms. The emission intensities can be corrected back to their levels before acceleration by using the ratios plotted in Fig. 5. The data shown in Fig. 3 were corrected in this way, and the results are plotted against radiation acceleration in Fig. 8. Comparison of this plot with uncorrected emissions in Fig. 3 shows that the scatter of points has decreased substantially. There is an initial decrease of about 20%, followed by a near-constant region in the range from about 30 to 160 cm/s^2, until shortly before the maximum acceleration is reached, where there is ∼20% drop for observations from the "out" leg, and an ∼20% increase for observations from the "in" leg. The emission intensity for the "out" leg starts decreasing above radiation acceleration levels of about 160 cm/s^2. This suggests that radiation acceleration acts to sweep sodium off the planet in this range, reducing the amount of sodium remaining on the planet. The opposite effect is seen for the "in" leg, where the intensity increases at radiation acceleration levels above about 160 cm/s^2, suggesting that radiation acceleration that slows sodium atoms relative to orbital velocity may lead to accumulation of sodium. A more detailed model of the effects of radiation acceleration may explain these differences.

The velocity changes expected for the sodium atoms as a result of radiation acceleration are large enough to be detected spectroscopically by their Doppler shift. However, the sodium velocity changes are always along the Mercury–Sun line, and only the vector component of the velocity that is in the Earth–Mercury line can be detected by and Earth-based observer. Since most of our observations were at phase angles not too far from 90°, the velocity vector seen in the Earth–Mercury line will generally be small (zero at 90° phase angle).

4.4. Comparison of the observed column densities of sodium with theoretical predictions

Assuming that the effects of solar radiation acceleration on emission intensity have been minimized by the correction, the average column density of sodium can be calculated by dividing the corrected emission intensities shown in Fig. 8 by the g-factor at the normalized true anomaly (9.712 photons/atom s). The results of this calculation are shown in Fig. 9, where the average column density of sodium seen in the 10 × 10-arcsec field of view is plotted against true anomaly angle. Smyth and Marconi (1995) modeled the variation of column density with true anomaly angle, taking into account energy exchange with the surface and assuming that sodium production varied as the inverse square of the distance from the Sun. Some insight into surface interaction can be found by comparing their model results with the observations, and this is done in Fig. 9, where plots taken from Fig. 15 of the Smyth and Marconi paper are overlaid. The scale for their calculated points was stretched so as to match the observed data. There are three overlays, each for a different value of β, the energy accommodation coefficient. A value of $\beta = 0$ implies that there is no interaction with the surface (perfectly elastic collisions), $\beta = 1$ implies that all the energy of the atom is lost upon contact with the surface (perfectly inelastic collisions), and $\beta = 0.5$ is an intermediate case. For true anomaly angles less than 180°, most of the data are close to the $\beta = 0$ line, except for a region just past the point of maximum radiation acceleration, implying little energy exchange with the surface. For true anomaly angles greater than 180°, the observations fall closer to the $\beta = 0.5$ line, except for the region near the point of maximum radiation acceleration, where there is a large jump. The slowdown of the sunward velocity of sodium atoms by radiation acceleration on the "in" leg of the orbit may enhance interaction with the surface.

As has been pointed out by Leblanc and Johnson (2003), the column abundances at perihelion and aphelion are of special interest, because at these points, the effect of solar radiation

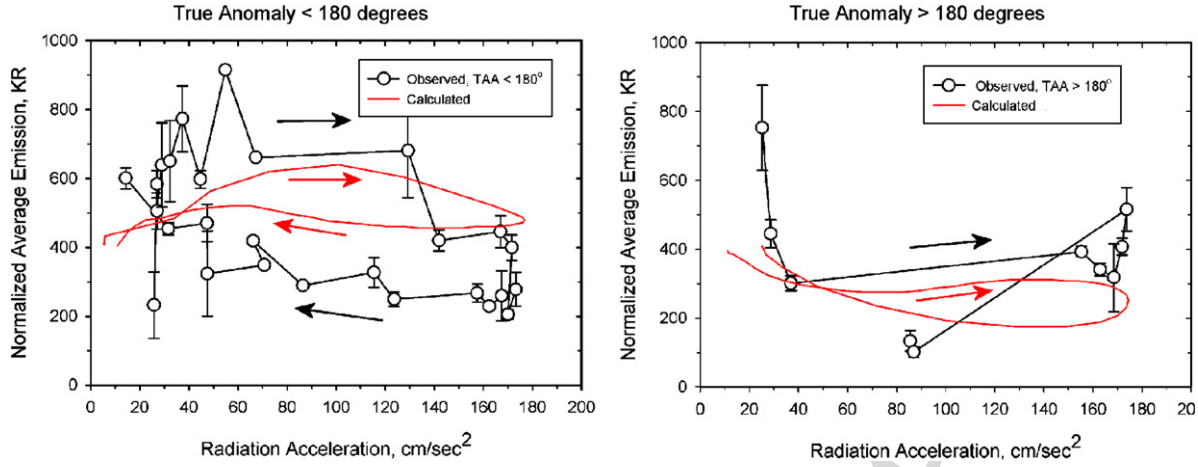

Fig. 7. The dusk terminator data shown in Fig. 3 are shown with overlay plots of the calculated emission. The left-hand part of the figure shows data for TAA values less than 180°, and the right-hand part shows data for TAA values greater than 180°. To get the calculated emission values, the ratios from Fig. 5 were multiplied by 400 kR so as to get an approximate match between the observed and calculated variations with radiation acceleration.

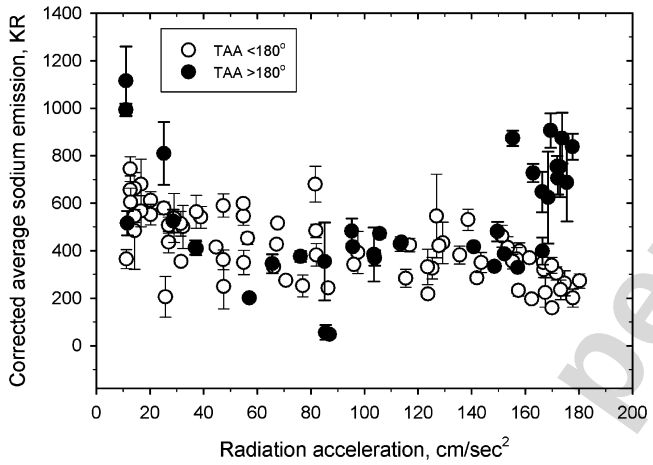

Fig. 8. The normalized sodium observations were corrected for the effect of solar radiation acceleration. The wide scatter of data points seen in the uncorrected emission values shown in Fig. 3 has diminished. A linear fit to the data yields an R-square value of 0.015 compared to 0.2 prior to the correction. An initial decrease is followed by a wide region of near-constant corrected emission, with changes near the end of the plot at maximum radiation acceleration. Near the end, there is a decrease of ∼20% for observations on the "out" leg of the orbit and an increase of a similar amount for observations on the "in" leg of the orbit. These effects may be real, or they may be artifacts of the simplified concept used for the correction. A more exact model may explain them.

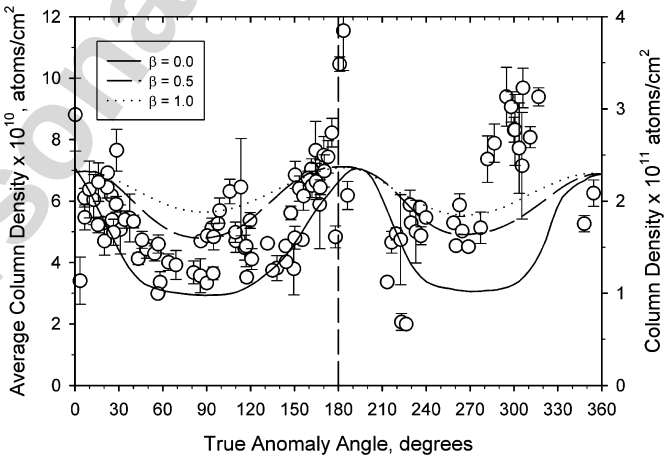

Fig. 9. Average column density data computed from the acceleration-corrected data of Fig. 8 is compared with predictions of Smyth and Marconi (1995). There are three overlays on this plot, taken from Fig. 15 of the Smyth and Marconi (1995) paper, in which they took into account radiation acceleration and the interaction of the sodium atoms with the surface. A value of $\beta = 0$ implies that there is no interaction with the surface, $\beta = 1$ implies that all the energy of the atom is lost upon contact with the surface, and $\beta = 0.5$ is an intermediate case. For true anomaly angles less than 180°, most of the data follow the $\beta = 0$ line, except for a region just past the point of maximum radiation acceleration, implying little energy exchange with the surface. For true anomaly angles greater than 180°, the observations fall closer to the $\beta = 0.5$ line, except for the region near the point of maximum radiation acceleration, where there is a large jump.

acceleration is negligibly small. There, the observed column abundances represent the steady state between source and sink processes without the perturbing effect of solar radiation acceleration. If both source and sink vary as the inverse square of radial distance, the column abundances should be the same at perihelion and aphelion. Fig. 9 shows that this is almost, but not quite, so. The average column abundance reaches a maximum value near aphelion. The column abundance is less at perihelion, such that the ratio of aphelion to perihelion column abundance is about 1.3. This suggests that the source rates for sodium atoms do not keep up with sink rates as Mercury comes closer to the Sun.

5. Summary and conclusions

Observations of the average sodium emission intensity from Mercury, measured over a time period from 1997 to 2003, were normalized to a constant true anomaly angle. The normalized emissions would be approximately proportional to the average sodium density of the atmosphere, provided there were no secondary effects of radiation acceleration. A plot of the normalized emission against solar radiation acceleration showed a general trend to lower values as radiation acceleration increased, but with very considerable scatter of the data. The

scatter was not random, but the result of a systematic variation, such that the normalized emission at a particular value of radiation acceleration took one or the other of two values, depending on the value of the true anomaly angle. We propose that this was the result of solar radiation acceleration changing the velocity of the sodium atoms, and consequently changing the solar continuum seen by the atoms. The emission intensity changes as a result. There is a positive feedback loop in the "out" leg of the orbit, with radiation acceleration increasing the emission intensity, and a negative feedback loop in the "in" leg of the orbit, such radiation acceleration decreases the emission intensity. The variation of normalized emission intensity with radiation acceleration could be fit approximately by assuming that the sodium atoms were accelerated by sunlight over a period of 1700 s. After correction for radiation acceleration, the plot of emission values versus radiation acceleration showed much less scatter. There appeared to be a general trend to lower values with increasing radiation acceleration, with most of the change occurring near minimum and maximum radiation acceleration. On the "out" leg of the orbit, where radiation acceleration increases the radial velocity, there is a decrease of emission near maximum radiation acceleration, suggesting that sodium is lost from the planet into the tail (Potter et al., 2002). However, the opposite effect is observed for the "in" leg of the orbit, where radiation acceleration decreases the absolute value of the radial velocity. There is an increase of emission near maximum radiation acceleration, suggesting that sodium is not lost, but rather redistributed.

The corrected emission values were used to compute average column densities and the results were compared with the theoretical predictions of Smyth and Marconi (1995). For true anomaly angles less than 180°, most of the data fall near the line predicted for perfectly elastic collisions with the surface ($\beta = 0$). This suggests that the energy exchange of sodium atoms with the Mercury surface is small on this leg of the orbit. For true anomaly angles greater than 180°, many of the data fall near the $\beta = 0.5$ line, while some fall completely above the predicted lines. This suggests a greater interaction with the surface on this leg of the orbit, where the absolute value of the radial velocity of sodium atoms is decreased by the effect of solar radiation acceleration.

Comparison of column densities at aphelion with those at perihelion is important, because at these two points, the effect of radiation acceleration is negligible. The column density at aphelion was larger than at perihelion by a factor of about 1.3, suggesting that the source processes for sodium do not keep up with loss processes as Mercury approaches the Sun.

The observations reported in this paper show that radiation acceleration can alter the emission intensity without any change in the column density of sodium. Consequently, the effect of radiation acceleration on emission intensities should be taken into account if column densities are to be calculated from emission intensities.

Acknowledgments

The data reported here were obtained at the McMath–Pierce Solar Telescope at the Kitt Peak National Observatory operated by the National Solar Observatory under agreement with the National Science Foundation. This work was supported by the NASA Planetary Astronomy program under Grants NNG05GF53G and NAG5-6991. We thank Claude Plymate of the McMath–Pierce Solar Telescope staff for his unstinting operational support, Trudy Tilleman for her faithful data processing support, and Francois Leblanc for his insightful comments.

References

Cremonese, G., Boehnhardt, H., Crovisier, J., Rauer, H., Fitzsimmons, A., Fulle, M., Licandro, J., Pollacco, D., Tozzi, G.P., West, R.M., 1997. Neutral sodium from Comet Hale–Bopp: A third type of tail. Astrophys. J. 490, L199–L202.

Domingue, D.L., Sprague, A.L., Hunten, D.M., 1997. Dependence of mercurian atmospheric column abundance estimations on surface-reflectance. Icarus 128, 75–82.

Ip, W.-H., 1990. On solar radiation-driven surface transport of sodium atoms at Mercury. Astrophys. J. 356, 675–681.

Killen, R.M., Sarantos, M., Potter, A.E., Reiff, P., 2004. Source rates and ion-recycling rates for Na and K at Mercury. Icarus 171, 1–19.

Leblanc, F., Johnson, R.E., 2003. Mercury's sodium exosphere. Icarus 164, 261–281.

Mallama, A., Wang, D., Howard, R.A., 2002. Photometry of Mercury from SOHO/LASCO and Earth. The phase function from 2 to 170 deg. Icarus 155, 253–264.

Potter, A.E., Morgan, T.H., 1987. Variation of sodium on Mercury with solar radiation pressure. Icarus 71, 472–477.

Potter, A.E., Killen, R.M., Morgan, T.H., 1999. Rapid changes in the sodium exosphere of Mercury. Planet. Space Sci. 47, 1141–1148.

Potter, A.E., Killen, R.M., Morgan, T.H., 2002. The sodium tail of Mercury. Meteorit. Planet. Sci. 37, 1165–1172.

Potter, A.E., Killen, R.M., Sarantos, M., 2006. Spatial distribution of sodium on Mercury. Icarus 181, 1–12.

Smyth, W.H., 1986. Nature and variability of Mercury's sodium atmosphere. Nature 323, 696–699.

Smyth, W.H., Marconi, M.L., 1995. Theoretical overview and modeling of the sodium and potassium atmospheres of Mercury. Astrophys. J. 441, 839–864.

Sprague, A.L., Kozlowski, R.W.H., Hunten, D.M., 1997. Distribution and abundance of sodium in Mercury's atmosphere, 1985–1988. Icarus 129, 506–527.

Ververka, J., Helfenstein, P., Hapke, B., Goguen, J.D., 1998. Photometry and polarimetry of Mercury. In: Mercury. Univ. of Arizona Press, Tucson, pp. 37–58.